Supplementary Information

Stable Electrode/Electrolyte Interfaces Regulated by Dual-Salt and Localized High-Concentration Strategies for High-Voltage Lithium Metal Batteries

Yingmeng Zhang,[†a,b] Lingxuan Zeng,[†a] Zaohui Ding,[a] Wei Wu,[a,b] Libo Deng[b] and Lei Yao[*a]

a. Shenzhen Key Laboratory of Special Functional Materials, Shenzhen Engineering Laboratory for Advanced Technology of Ceramics, Guangdong Research Center for Interfacial Engineering of Functional Materials, College of Materials Science and Engineering, Shenzhen University, Shenzhen, 518060, China. E-mail: lyao@szu.edu.cn (Prof. L. Yao)

b. College of Chemistry and Environmental Engineering, Shenzhen University, Shenzhen, 518060, China

1. Experimental Section

1.1. Configurations of electrolytes

The high concentration electrolyte (HCE) was prepared by dissolving different lithium salts in 1,2-dimethoxyethane (DME) solvent. And localized high concentration electrolyte (LHCE) was prepared by dissolving different lithium salts in the mixture of 1,2-dimethoxyethane (DME) as solvent and 1,1,2,2-tetrafluoroethyl-2,2,3,3-tetrafluoropropyl ether (TTE) as the diluent.

The detailed compositions of the as-prepared electrolytes with abbreviations are listed in **Table S1**, where HCE-LiFSI is referred to 4.0 M lithium bis(fluorosulfonyl)imide (LiFSI) in DME, HCE-LiDFOB is referred to 4.0 M lithium difluoro(oxalato)borate (LiDFOB) in DME, and HCE-dual is referred to 2 M LiFSI and 2 M LiDFOB in DME, while LHCE-LiFSI is referred to 1.0 M LiFSI in DME/TTE (V_{DME}:V_{TTE}=1:3), LHCE-LiDFOB is referred to 1.0 M LiDFOB in DME/TTE (V_{DME}:V_{TTE}=1:3), and LHCE-dual is referred to 0.5 M LiFSI and 0.5 M LiDFOB in DME/TTE (V_{DME}:V_{TTE}=1:3).

The commercial electrolytes used as comparison in this article were purchased and directly used, which was 1 M $LiPF_6$ in DMC/EC (7:3 by volume ratio).

1.2. Materials characterizations

The morphology was analyzed by field-emission scanning electron microscope (FESEM, Hitachi SU-70, Japan) operating at 5 KV, and transmission electron microscope (TEM, JEOL-F200, Japan) operating at 200 KV. The chemical states of

the elements were identified by X-ray photoelectron spectroscopy (XPS, ESCALAB 250Xi, Thermo Scientific, United States). The Raman measurements were measured on a Raman microscope (Dxr2xi, Thermo Scientific, United States).

1.3. Electrochemical measurements

The electrochemical performance was evaluated with CR2025 coin-type cell configuration at room temperature. The polypropylene (PP) microporous membrane (Celgard 2500) was supplied as the separator. And 50 μL of electrolyte with different composition was dropped into each coin cell. The Li||Li, Cu||Li and NCM811||Li half cells were assembled, in which Li foils were used as the reference and counter electrodes. For the NCM811||Li half cells, $LiNi_{0.8}Co_{0.1}Mn_{0.1}$ (NCM811) was applied as the active material for cathode. The cathodes were prepared with active materials, carbon black, and polyvinylidene fluoride (PVDF) binder in a mass ratio of 8:1:1 mixed in N-methyl pyrrolidone (NMP) and casted on Al foil. After drying at 60 °C under vacuum overnight, the prepared cathode was cut into discs with diameter of 14 mm, and the typical mass loading is about 8.458 mg cm^{-2}. The pouch cell (4 × 6 cm scale) was configurated by NCM811 as the cathode and Li-Mg alloy as anode (Li: 16wt%, Mg: 84wt%). The N/P ratio (negative electrode capacity/positive electrode capacity) for the full cell was maintained at approximately 1.26. The specific capacity of the full cell was determined based on the mass of the cathode. For comparison, NCM811||Li half cell was assembled using dual-salt LHCE (LiTFSI and LiDFOB) electrolyte, where 0.5 M LiTFSI and 0.5 M LiDFOB dissolved in DME/TTE (V_{DME}:V_{TTE}=1:3). The LCO||Li cell was also configurated by $LiCoO_2$ as cathode

(areal density: 2.2 mg cm^{-2}), Li foil as anode and LHCE-dual as electrolyte.

Linear sweep voltammetry (LSV) was conducted at a scan rate of 1.0 mV s^{-1} between 2.0 and 6.0 V using an electrochemical station (CHI760E, China). Cyclic voltammetry (CV) was measured at a scan rate of 0.01 mV s^{-1} between 3.0 and 4.3 V on an electrochemical station (CHI760E, China). The electrochemical impedance spectroscopy (EIS) was collected by CHI760E electrochemical station in the frequency range of 100 kHz to 0.01 Hz, which was obtained at an AC potential amplitude of 5 mV around the open circuit before the electrochemical performance testing. Voltage profiles and long-term cycling performances were conducted on a NEWARE CT-ZWJ-4'S-T-1U battery testing system. Li||Li half cells were tested at different current densities with a capacity of 1.0 mAh cm^{-2}. Cu||Li half cells were measured at a current density of 0.5 mA cm^{-2} with a capacity of 0.5 mAh cm^{-2}.

1.4. Electrode Characterization.

The composition and morphology of the cycled electrodes were observed by disassembling the half cells in the Ar-filled glovebox at room temperature and drying overnight for XPS, SEM and TEM.

1.5. Ionic Models and Computational Methodology

Quantum chemistry calculations were first performed to optimize molecular geometries of DFOB anion using the Gaussian 16 package at B3LYP/6-311+G(d,p) level of theory. The atomic partial charges on DFOB anion were calculated using the ChelpG method at the same level of theory (the B3LYP hybrid functional and the 6-311+G(d,p) basis set). The atomistic force field parameters for all ions and molecules

are described by the AMBER format and are taken from previous work.[1] The cross-interaction parameters between different atom types are obtained from the Lorentz-Berthelot combination rule.

Atomistic simulations were performed using GROMACS package with cubic periodic boundary conditions. The detailed simulation system compositions are listed in **Table S2**. The equations for the motion of all atoms were integrated using a classic Verlet leapfrog integration algorithm with a time step of 1.0 fs. A cutoff radius of 1.6 nm was set for short-range van der Waals interactions and real-space electrostatic interactions. The particle-mesh Ewald (PME) summation method with an interpolation order of 5 and a Fourier grid spacing of 0.20 nm was employed to handle long range electrostatic interactions in reciprocal space. All simulation systems were first energetically minimized using a steepest descent algorithm, and thereafter annealed gradually from 600 K to room temperature (300 K) within 10 ns. All annealed simulation systems were equilibrated in an isothermal-isobaric (NPT) ensemble for 20 ns of physical time maintained using a Nosé-Hoover thermostat and a Parrinello-Rahman barostat with time coupling constants of 0.4 and 0.2 ps, respectively, to control the temperature at 300 K and the pressure at 1 atm. Atomistic simulations were further performed in a canonical ensemble (NVT) for 50 ns, and simulation trajectories were recorded at an interval of 100 fs for further structural and dynamical analysis.

After extensive atomistic simulations, the representative solvation structures were extracted from simulation trajectories, and are used as starting configurations to

perform quantum chemistry calculations at the same level of theory (the B3LYP hybrid functional and the 6-311+G(d,p) basis set) to calculate HOMO and LUMO energies.

Figures

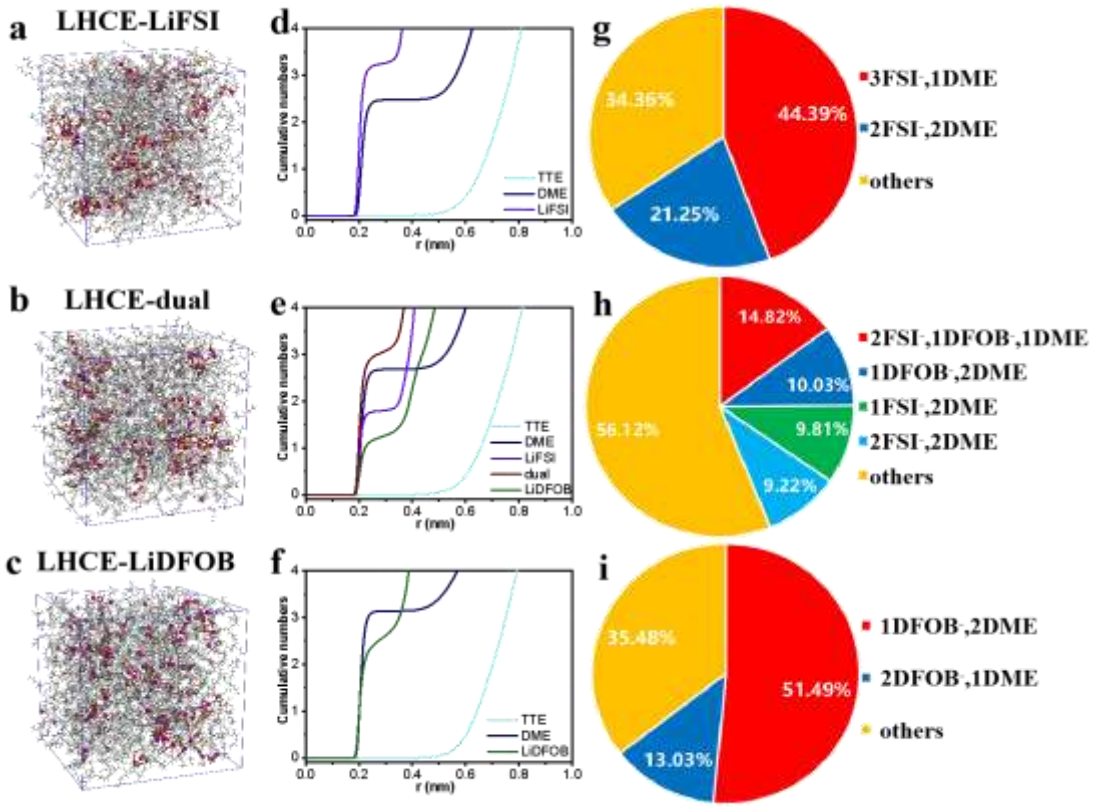

Figure S1 Molecular dynamics simulation of LHCE-LiFSI, LHCE-LiDFOB and LHCE-dual: (a-c) MD simulation snapshots. (d-f) Li^+ radial distribution function. (g-i) Solvation structures and composition.

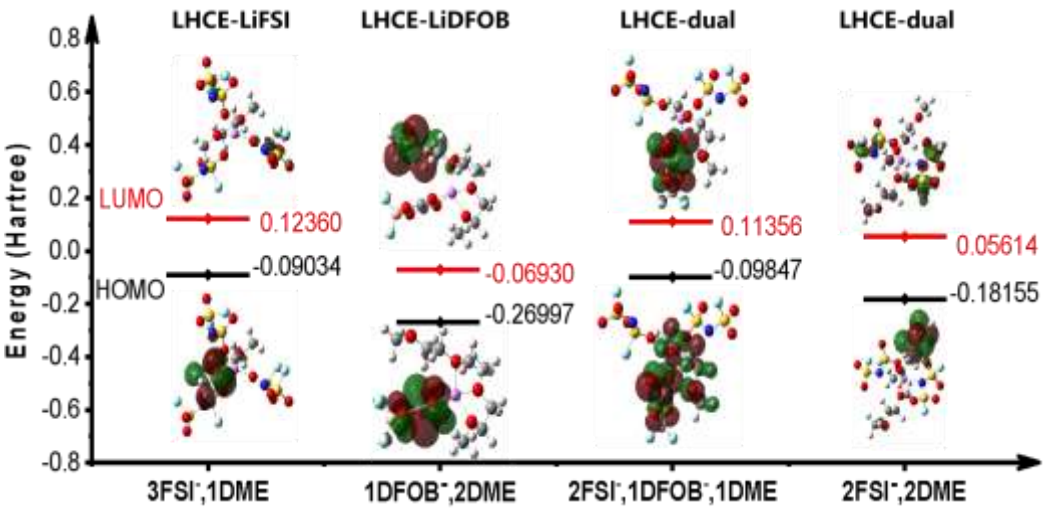

Figure S2 LUMO/HOMO energy levels of four representative Li^+ solvation structures: Li^+-3FSI^--1DME for LHCE-LiFSI, Li^+-1$DFOB^-$-2DME for LHCE-LiDFOB, Li^+-2FSI^--1$DFOB^-$-1DME and Li^+-2FSI^--2DME for LHCE-dual.

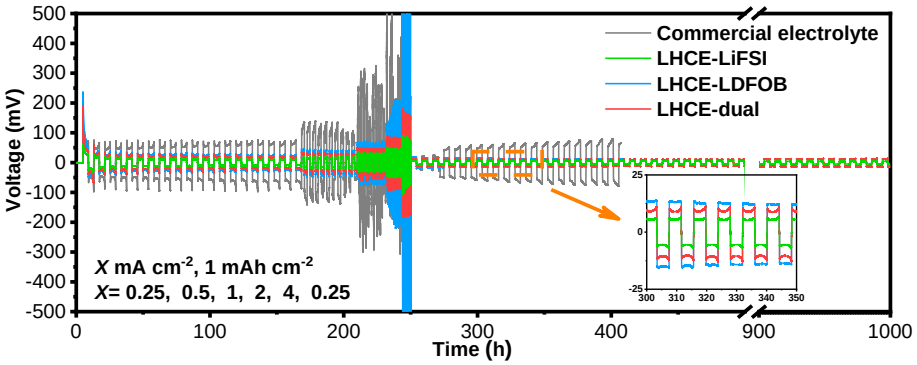

Figure S3 Rate performance comparisons among LHCE-LiFSI, LHCE-LiDFOB and LHCE-dual as well as commercial electrolyte in symmetrical Li||Li cells with a consistent areal capacity of 1 mAh cm^{-2} in different current densities.

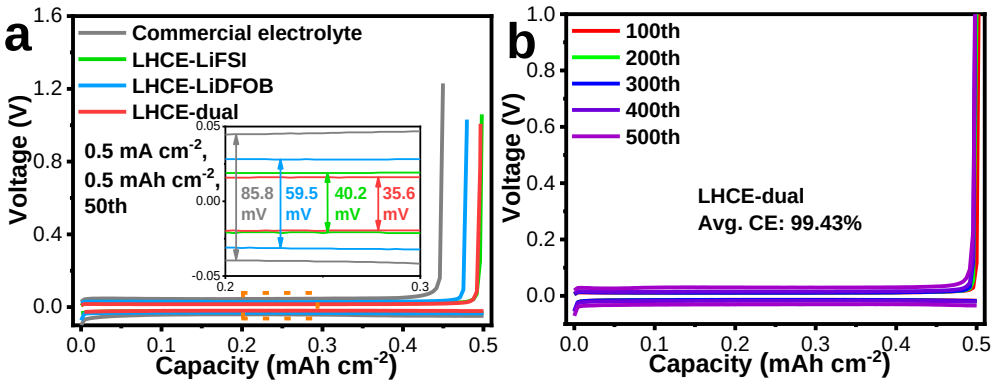

Figure S4 Corresponding charge-discharge profiles in Li||Cu cells at 0.5 mA cm^{-2} with an areal capacity of 0.5 mAh cm^{-2}.

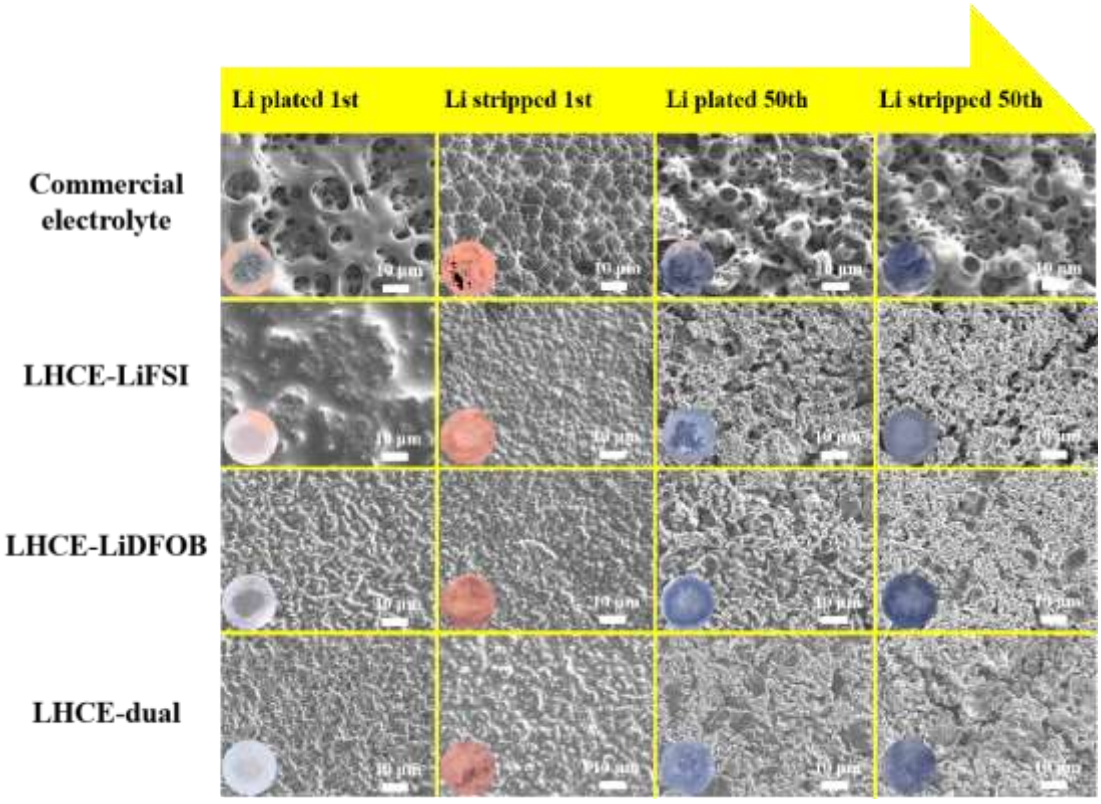

Figure S5 SEM images of the Cu surfaces after Li plating/stripping tests in Li||Cu cells (insert, the corresponding digital photos of Cu foils).

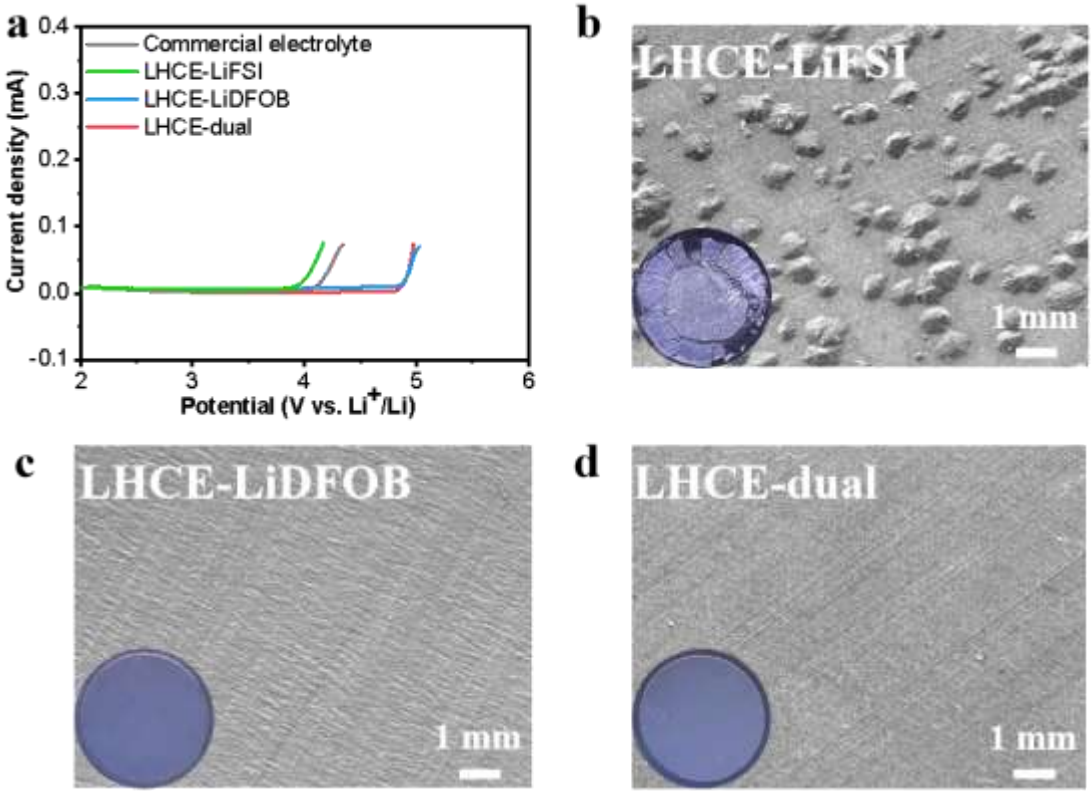

Figure S6 (a) LSV profile comparisons among LHCE-LiFSI, LHCE-LiDFOB and LHCE-dual as well as commercial electrolyte in Li||Al cells at a scan rate of 1.0 mV s^{-1} between 2.0 and 6.0 V. (b-d) SEM images of the Al surfaces after LSV testing (insert, the corresponding digital photos of Al foils).

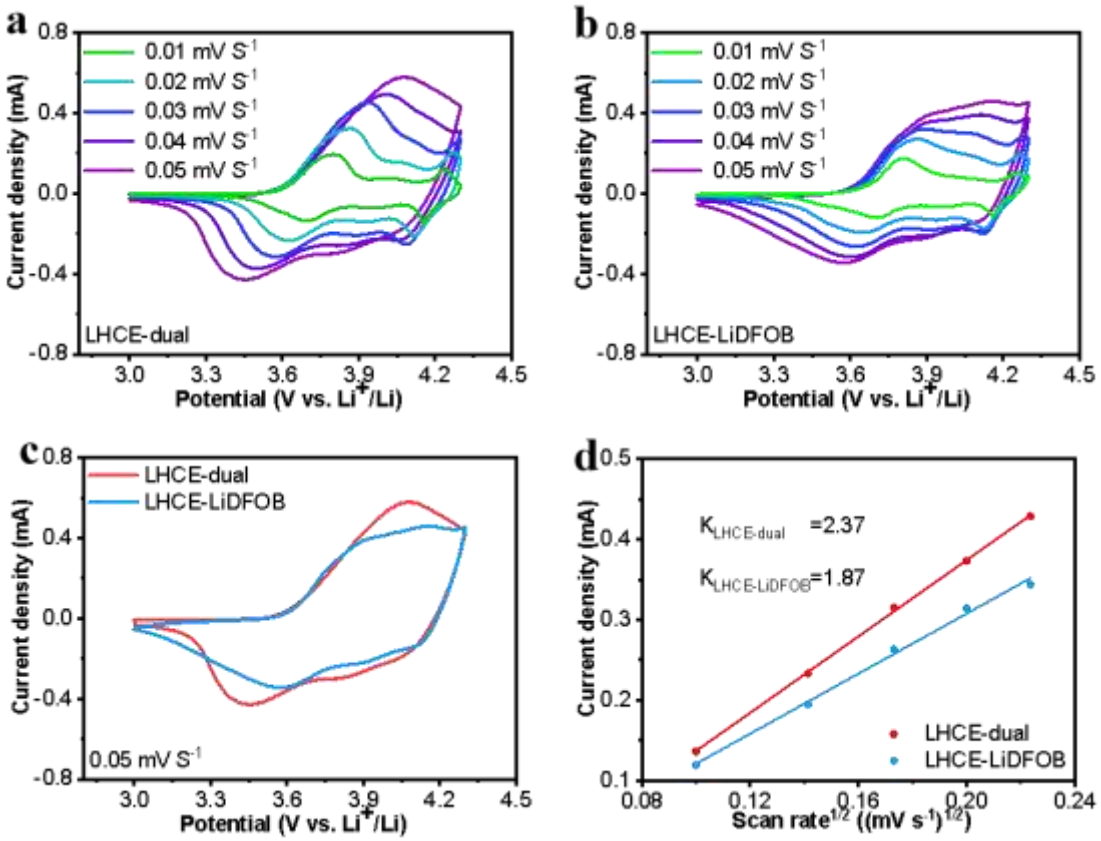

Figure S7 CV profiles of NCM811||Li cells in LHCE-dual (a) and LHCE-LiDFOB (b). (c) LSV profile comparisons between LHCE-dual and LHCE-LiDFOB. (d) Linear fitting plots of the peak current as a function of scan rate of CV curves.

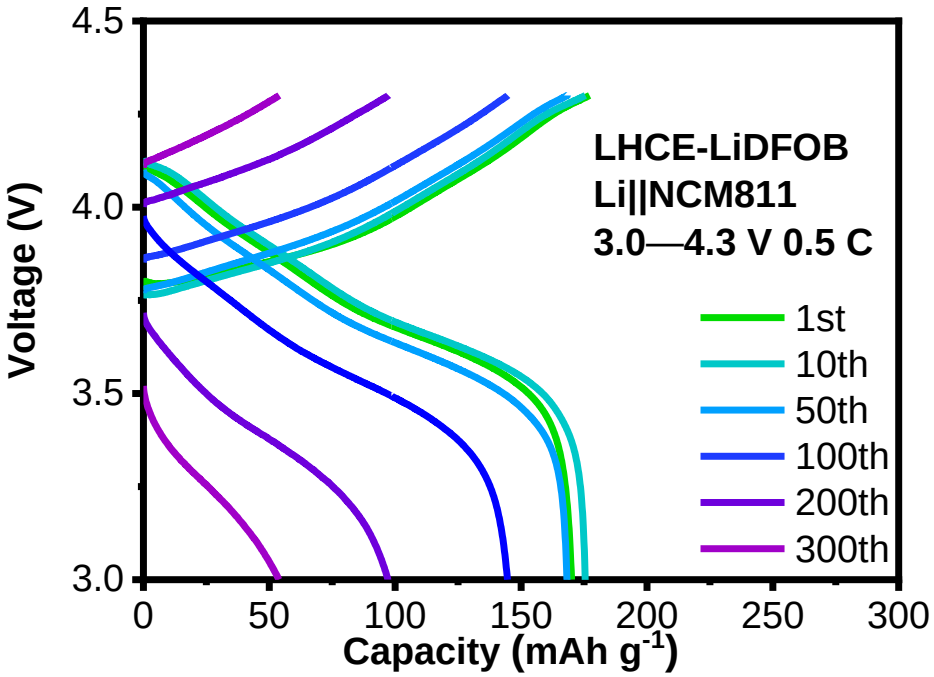

Figure S8 The charge-discharge curves of LHCE-LiDFOB cycling at 0.5 C between 3.0 and 4.3 V.

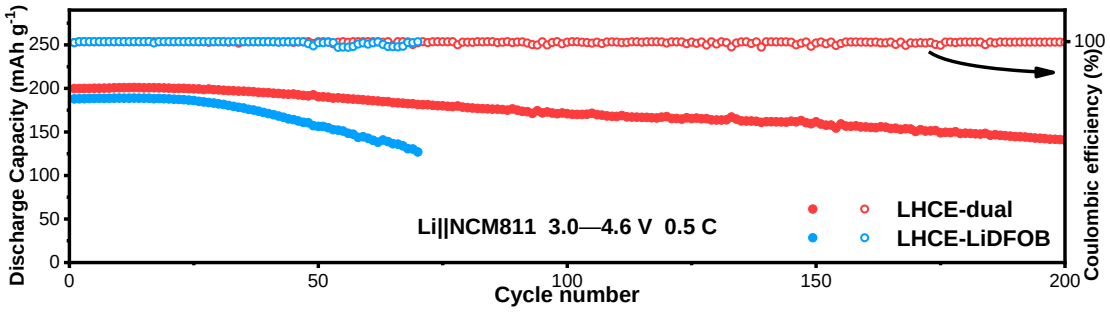

Figure S9 Long-term cycling performance comparisons among LHCE-LiDFOB and LHCE-dual at 0.5 C in a broader voltage window of 3.0-4.6 V.

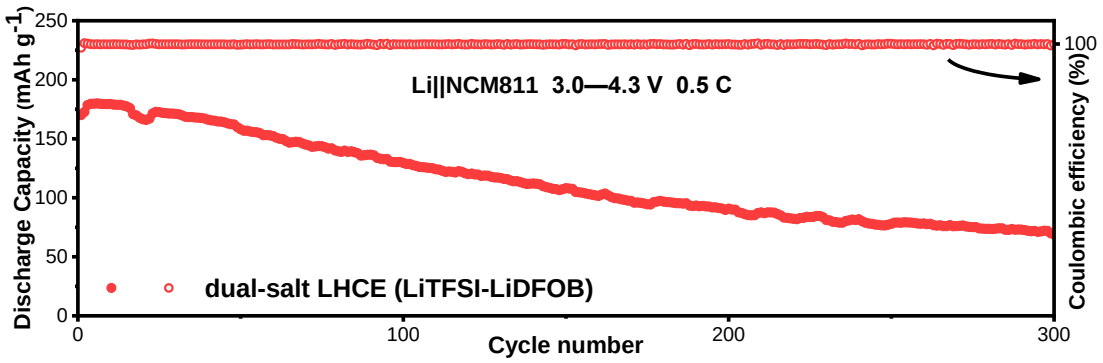

Figure S10 Long-term cycling performance of NCM811||Li cell in dual-salt LHCE (LiTFSI-LiDFOB) electrolyte at 0.5 C between 3.0 and 4.3 V.

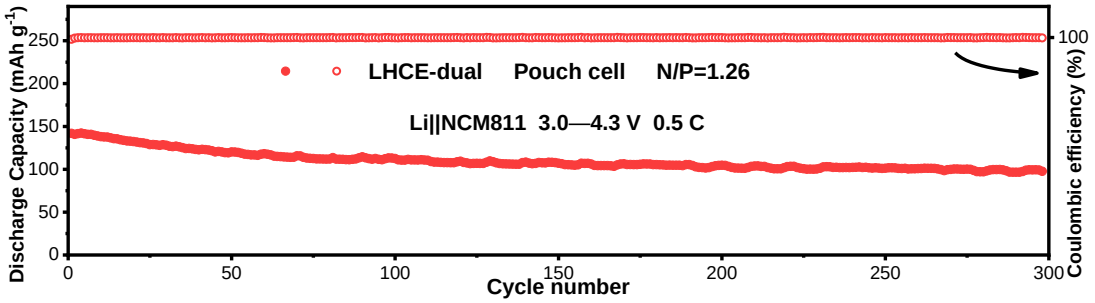

Figure S11 Long-term cycling performance of the NCM811||Li pouch cell at 0.5 C between 3.0 and 4.3 V.

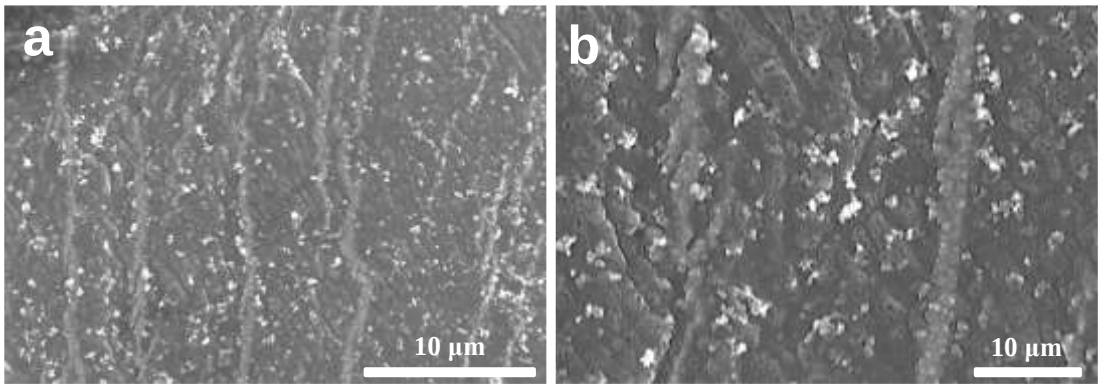

Figure S12 SEM images of Li metal anode disassembled from cycled NCM811||Li cell after testing at 0.5 C between 3.0 and 4.3 V for 100 cycles.

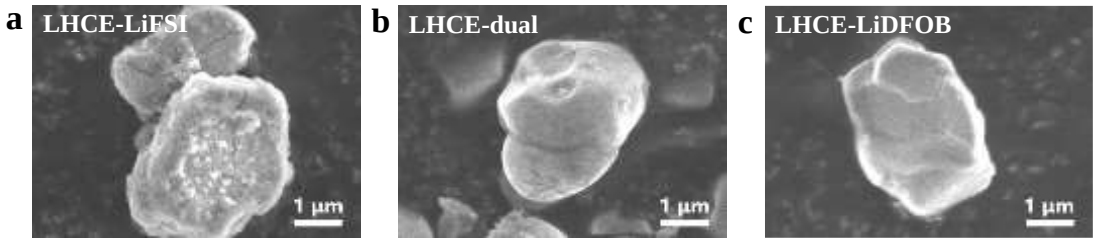

Figure S13 SEM images of NCM811 cathode nanoparticles disassembled from NCM811||Li cells after cycling.

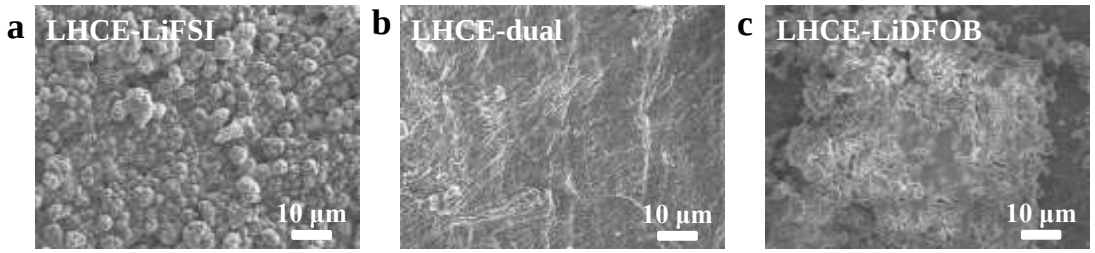

Figure S14 Top-view SEM images of Li metal anodes disassembled from NCM811||Li cells after cycling.

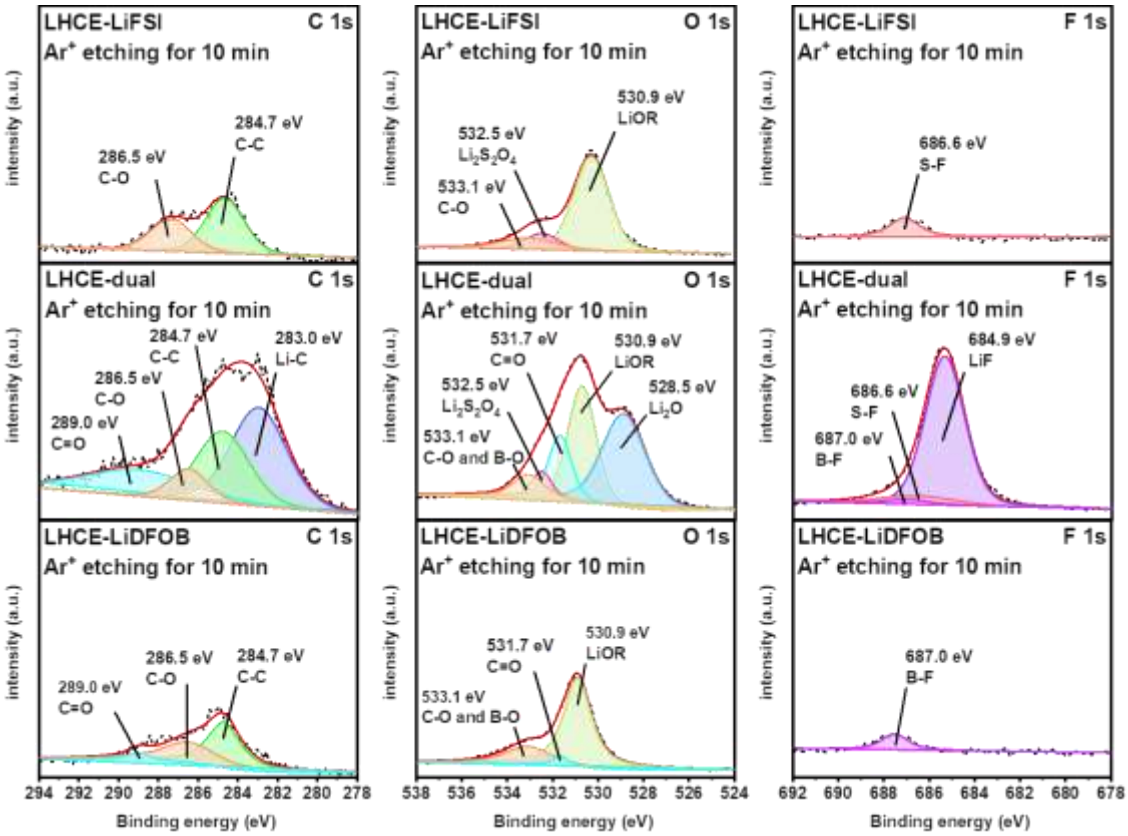

Figure S15 XPS analysis with Ar^+ etching for 10 min of Li metal anodes disassembled from NCM811||Li cells after cycling.

Table S1 Compositions of prepared electrolyte systems.

Electrolyte	Composition
Commercial electrolyte (CE)	1 M LiPF6 / DMC-EC (V_{DMC}:V_{EC}=7:3)
HCE-LiFSI	4 M LiFSI / DME
HCE-LiDFOB	4 M LiDFOB / DME
HCE-dual	2 M LiFSI+2 M LiDFOB / DME
LHCE-LiFSI	1 M LiFSI / DME-TTE (V_{DME}:V_{TTE}=1:3)
LHCE-LiDFOB	1 M LiDFOB / DME-TTE (V_{DME}:V_{TTE}=1:3)
LHCE-dual	0.5 M LiFSI+0.5 M LiDFOB / DME-TTE (V_{DME}:V_{TTE}=1:3)

Table S2 Compositions for molecular dynamics simulation

	LHCE-LiFSI	LHCE-dual	LHCE-LiDFOB
Li^+	100	100	100
FSI^-	100	50	0
$DFOB^-$	0	50	100
DME	240	240	240
TTE	680	680	680
Total atom	17080	17080	17080
Volume	$(6.0477\ nm)^3$	$(6.0507\ nm)^3$	$(6.0428\ nm)^3$

Table S3 Electrochemical performance comparisons between LHCE-dual and recently reported electrolytes.

Batteries	Electrolytes	voltage /V	Cycle performance/(mAh·g^{-1})	Ref.
NCM811||Li	LHCE-dual	3.0 - 4.3	127.46 (300 cycles at 0.5 C)	This work
NCM811||Li	LHCE-dual	3.0 - 4.6	140.57 (200 cycles at 0.5 C)	This work
NCM811||Li	FEC/ETFEC-based	3.0 - 4.6	~145 (225 cycles at 1.0 C)	2
NCM811||Li	TMSTFA additive	3.0 - 4.3	149 (200 cycles at 1.0 C)	3
NCM811||graphite	LiDFOB additive	2.8 - 4.6	~180 (100 cycles at 0.5 C)	4
NCM523||Li	ADFN	3.0 - 4.3	142 (200 cycles at 1.0 C)	5
NCM523||Li	TEH-2m-LiTD+10 wt% FEC	3.0 - 4.6	~160 (200 cycles at 1.0 C)	6
NCA||Li	LiF nanobox in electrolyte	2.7–4.4	149 (200 cycles at 1.0 C)	7
NCM811||Li	DME+TTE+FEC	3.0 - 4.2	~150 (150 cycles at 0.5 C)	8
NCM523||Li	DH(3/5)-	3.0 - 4.3	~135 (200 cycles at 0.5 C)	9

	1.65M-LiFSI			
NCM523||Li	**LHCE with HFE**	**3.0 - 4.3**	**~120 (140 cycles at 0.5 C)**	**[10]**
LCO||Li	**LHCE with DFEC**	**3.0 - 4.5**	**~140 (200 cycles at 0.5 C)**	**[11]**

References

1. Y.-L. Wang, F. U. Shah, S. Glavatskih, O. N. Antzutkin and A. Laaksonen, *The Journal of Physical Chemistry B*, 2014, **118**, 8711-8723.
2. W. N. Zhang, T. Yang, X. B. Liao, Y. Song and Y. Zhao, *Energy Storage Mater*, 2023, **57**, 249-259.
3. S. Jiang, X. Xu, J. Y. Yin, H. H. Wu, X. Q. Zhu and Y. F. Gao, *Acs Appl Mater Inter*, 2022, **14**, 38758-38768.
4. Q. Zhao, Y. Wu, Z. W. Yang, D. P. Song, X. L. Sun, C. Wang, L. Yang, Y. Zhang, J. Gao, T. Ohsaka, F. Matsumoto and J. F. Wu, *Chem Eng J*, 2022, **440**.
5. T. L. Zheng, J. W. Xiong, X. T. Shi, B. Y. Zhu, Y. J. Cheng, H. B. Zhao and Y. G. Xia, *Energy Storage Mater*, 2021, **38**, 599-608.
6. S. S. Lin, H. M. Hua, P. B. Lai and J. B. Zhao, *Adv Energy Mater*, 2021, **11**, 2101775.
7. Y. H. Tan, G. X. Lu, J. H. Zheng, F. Zhou, M. Chen, T. Ma, L. L. Lu, Y. H. Song, Y. Guan, J. X. Wang, Z. Liang, W. S. Xu, Y. G. Zhang, X. Y. Tao and H. B. Yao, *Adv Mater*, 2021, **33**, 2102134.
8. Y. Lee, T. K. Lee, S. Kim, J. Lee, Y. Ahn, K. Kim, H. Ma, G. Park, S. M. Lee, S. K. Kwak and N. S. Choi, *Nano Energy*, 2020, **67**, 104309.
9. S. S. Lin, H. M. Hua, Z. S. Li and J. B. Zhao, *Acs Appl Mater Inter*, 2020, **12**, 33710-33718.
10. D. J. Yoo, S. Yang, K. J. Kim and J. W. Choi, *Angew Chem Int Edit*, 2020, **59**, 14869-14876.
11. C. H. Luo, Q. Liu, X. S. Wang, Y. Tian, Z. F. Liu, F. Y. Kang and B. H. Li, *Nano Energy*, 2023, **109**, 108323.